28

Synchrotron Radiation and Nanotechnology for Stem Cell Research

Alessandra Giuliani, Fabrizio Fiori, Adrian Manescu,
Vladimir S. Komlev, Chiara Renghini and Franco Rustichelli
Polytechnic University of Marche, Department SAIFET – Physical Sciences Section, Ancona
Italy

1. Introduction

Stem cell based tissue engineering therapies involve the administration of manipulated stem cell populations with the purpose of repairing and regenerating damaged or diseased tissue. Currently available methods of monitoring transplanted cells are quite limited. The monitoring of stem cell therapy outcomes requires the development of non-destructive strategies capable to identify the location, magnitude, and duration of cellular survival and fate. The recent development of imaging techniques offers great potential to address these critical issues by non-invasively tracking the fate of the transplanted cells. This chapter offers a focused presentation of some examples of the use of imaging techniques connected to the nanotechnological world in research areas related to stem cells. In particular, investigations concerning human stem cell treatment of Duchenne muscular dystrophy in animal models, cellular therapy to generate new myocardium in infarcted rat heart, bioscaffolds for cell proliferation driving to form bone tissue will be discussed.

Tissue engineering and regenerative medicine represent an emerging research area that promises new therapeutic techniques for the repair and replacement of tissues and organs that have lost functions due to ageing, disease, damage, and congenital defects (Langer & Vacanti, 1999; Atala, 2005; Jones & Hench, 2003). Clinical applications have already begun to repair a wide variety of tissues, such as blood, skin, cornea, cartilage, and bone.

Imaging techniques are playing an increasingly important role in the rigorous characterization of biomaterial properties and function. Sophisticated 2D imaging technologies have been developed to complement histological evaluation and probe complex biological events occurring at the interface between tissues and biomaterials (Boskey & Pleshko Camacho, 2007; Campbell & Kim, 2007). However, there is a clear need for high resolution 3D imaging technologies that reveal the spatial distribution of regenerated tissues forming in vitro and in vivo conditions.

Moreover, for regeneration of vascularized tissues such as bone or muscle, the ability to quantify 3D vascular in-growth would be tremendously valuable, particularly for studies exploring the potential to enhance regeneration via therapeutic angiogenesis strategies (Silva & Mooney, 2007). The imaging modality that has been most extensively applied for this purpose, particularly for bone tissue engineering studies (Mastrogiacomo et al., 2004;

Komlev et al., 2006; Papadimitropoulos et al., 2007; Eniwumide et al., 2007), is high resolution X-ray computed tomography (CT). CT provides rapid reconstruction of 3D images and quantitative volumetric analysis of X-ray attenuating materials or tissues. In the perspective of clinical translation of stem cell research, it would be advantageous to develop new techniques to detect donor cells after transplantation to track their fate and thus better understand their role in regeneration of damaged and diseased tissues.

Several groups have reported on successful labelling of mesenchymal pig (Hill et al., 2003) and mouse (Hoehn et al., 2002) embryonic stem cells with nanoparticles of iron oxide (SPIO). These particles are used as contrast agents for magnetic resonance imaging (MRI) (Arbab et al., 2003; Wang et al., 2001). It appears that cells that are able to incorporate SPIO intracellularly are readily detectable with MRI allowing in vivo tracking of such "tagged" cells (Bulte et al., 2002). MRI can provide a non-invasive and repeated three-dimensional visualization of transplanted "tagged" stem cells in organs, making it particularly attractive for imaging studies (Nuzzo et al., 2002).

The aim of this Chapter is to present recent progress obtained by using innovative and non-invasive imaging techniques, involving nanotechnologies in research areas related to stem cells. In particular, the authors will provide some examples of studies concerning human stem cell treatment of Duchenne muscular dystrophy in animal models, cellular therapy to generate new myocardium in infarcted rat heart, bioscaffolds for cell proliferation driving to form bone tissues.

The interest will be focused on X-ray computed microtomography (micro-CT), that is an imaging technique similar to conventional CT systems usually employed in medical diagnostics but with the main difference that in micro-CT a spatial resolution in the order of a few hundred nanometers can be achieved (against about 0.5 mm in CT). On the other hand, of course, such a high spatial resolution can be obtained only for reduced size samples (a few mm^3). In particular, by using synchrotron radiation, available at some European Large Scale Facilities like ESRF - Grenoble, PSI/SLS - Zurich, BESSY HZB - Berlin, HASYLAB - Hamburg and ELETTRA - Trieste, it is possible to couple high spatial resolution to high signal-to-noise ratio (Nuzzo et al., 2002; Salomé et al., 1999). Furthermore, with respect to conventional laboratory sources, the advantages of X-rays produced at synchrotron radiation sources also include a very high photon flux and a tunable-energy monochromatic beam with high coherency, in parallel beam geometry.

In conclusion, the authors will evidence that non-destructive 3D imaging techniques, such as micro-CT, are increasingly providing a powerful set of quantitative tools to aid in the development and evaluation of porous biomaterials and new approaches to engineering tissues and organs. Emphasis will be given to the fact that the key advantage of micro-CT imaging is that this method, as well as MRI, may be applicable to monitoring the stem cell homing, after cell labelling with iron oxide nanoparticles. On the other hand, when working on biopsies of small sizes (few millimeters) or small animals, micro-CT has an appreciably higher spatial resolution as compared to magnetic resonance imaging, which, in turn, has the advantage to be applicable to human body.

Micro-CT will be also shown to be a good technique for 3D studies of bioscaffolds for tissue engineering, also allowing the 3D visualization, as well as quantitative evaluations, of features very difficult to be detected by other imaging methods, such as the vascularization network in engineered bone tissue.

2. X-ray Microtomography: Outline of the technique

A revolutionary discovery in the field of medical imaging occurred at the beginning of the 1970s when the first equipment for X-rays Computed Tomography (CT) was developed. This method of imaging avoids several important limitations of conventional X-ray radiology. The impact of the CT technique has been revolutionary, enabling to view internal sample details with unprecedented precision and in a non-destructive way. Furthermore it achieves a contrast discrimination up to one thousand times better than conventional radiography (Claesson, 2001).

Tomography refers to the cross-sectional imaging of an object from either transmission or reflection data collected by illuminating the object from many different directions (Kak & Slaney, 2001). Although the first application was in diagnostic medicine, there are indeed numerous nonmedical imaging applications. This methodology is applied to the mapping of underground resources via cross borehole imaging, to some specialized cases of cross-sectional imaging for nondestructive testing, to the determination of the brightness distribution over a celestial sphere, to three-dimensional imaging with electron microscopy, etc. (Kak & Slaney, 2001).

Fundamentally, tomography employs X-rays to form images of objects based on their attenuation coefficient. Tomographic imaging deals with reconstructing an image from its projections.

The solution to the problem of how to reconstruct a function from such projections dates back to the paper published by Radon in 1917 and it was exploited with Hounsfield's invention of the x-ray computed tomographic scanner for which the same Hounsfield received a Nobel prize in 1972.

Given the enormous success of X-ray computed tomography, it is not surprising that in recent years much attention has been focused on extending this image formation technique to nuclear medicine and magnetic resonance, on one hand, and ultrasound and microwaves on the other (Kak & Slaney, 2001).

Computed X-ray microtomography (micro-CT) is similar to conventional CT systems usually employed in medical diagnoses and industrial applied research. Unlike these systems, which typically have a maximum spatial resolution of about 0.5 mm, advanced micro-CT is capable of achieving a spatial resolution up to 0.1 microns (Weitkamp et al. 2010), i.e. about three orders of magnitude lower. Such a high spatial resolution can be obtained only for samples of reduced size i.e. for dimensions in the range of a few cubic millimeters. Synchrotron Radiation allows achieving high spatial resolution images to be generated with high signal-to-noise ratio (Nuzzo et al., 2002; Salomé et al., 1999). Use of X-rays delivered by Synchrotron Facilities has several advantages compared to X-rays produced by Laboratory or Industrial sources. These include: (i) a high photon flux which permits measurements at high spatial resolution; (ii) the X-ray source is tunable, thus allowing measurements at different energies; (iii) the X-ray radiation is monochromatic, which eliminates beam hardening effects; and (iv) parallel beam acquisition allows the use of exact tomographic reconstruction algorithms. In addition, Synchrotron Radiation allows acquisition of volumes at different energies and volume subtraction to enhance contrast. Because of this variability, it is possible to enables digital image processing of micro-CT data in order to maximize contrast between neighboring voxels in the image and to increase the range of attenuation values of the entire volume. This variability in materials and acquisition methods leads to a wide range of grayscale values (corresponding to different X-ray absorption coefficients) within and among data sets (Ashbridge et al., 2003).

The spatial resolution of the CT image is dependent on the number of parallel beam projections and the number of data points in each projection. A larger data set means a more detailed description of the depicted object and hence more pixels and of smaller dimensions, i.e. better spatial resolution.

An important issue is the choice of spatial resolution versus overall sample size. Ideally, the specimen should absorb about 90 % of the incident radiation along the most radio-opaque path to obtain the best signal to noise ratio in the reconstructed image. In a homogeneous sample, absorbing 90 % of the incident radiation, the quantity $\mu(\lambda)x$ (where λ is the X-ray wavelength, $\mu(\lambda)$ is the linear attenuation coefficient of the sample for this wavelength, and x is the sample thickness), should be approximately 2. To satisfy this condition the sample thickness and/or the X-ray energy should be optimized.

In both three-dimensional (3D) conventional CT and micro-CT, hundreds of two-dimensional (2D) projection radiographs of the specimen are taken at several different angles. The information contained in each radiograph is a projection of the absorption density distribution in the sample along the direction of X-ray beam onto the plane perpendicular to the direction of the X-ray beam propagation. If the sample is then imaged several times in different orientations, 3D (volume) information on the sample structure can be obtained by using computer algorithms. This process, referred to as "tomographic image reconstruction", consists in solving an inverse problem to estimate an image from its line integrals on different directions, in 2D, and the problem is theoretically equivalent to the inversion of the Radon Transform of the image.

In practice, there are two major classes of reconstruction algorithms that use fundamentally different approaches to accomplish this conversion (Paulus et al., 2000): (i) transform-based methods using analytic inversion formulae, and (ii) series expansion methods based on linear algebra. Fourier-transform-based algorithm is commonly used in micro-CT.

An alternative approach to image reconstruction involves the use of iterative reconstruction algorithms. These algorithms start with an initial estimate of the 2D matrix of attenuation coefficients (Webb, 2003). By comparing the projections predicted from this initial estimate with those that are actually acquired, changes are made to the estimated matrix. This process is repeated for each projection in a first step, and, in a second step, also for the whole dataset until the residual error between the measured data and estimated matrix falls below a predesignated value. Iterative schemes are used relatively sparingly in standard CT scanning.

3D renderings of the data obtained after the reconstruction may be made by electronically stacking up the slices. These 3D renderings may be also sectioned in arbitrary ways and could be planed, zoomed and rotated to better locate individual details. While the slice image and 3D renderings are very useful for making qualitative observations of an internal concrete structure, the real benefit is the quantitative information that can be extracted from the 3D data sets (Ohgughi et al., 1989).

Different methods may be applied to extract quantitative architectural parameters from the tomographic images. In the field of bone research, different ways have been proposed to quantify bone micro-architecture. The 3D Mean Intercept Length (MIL) method may provide estimation of trabecular thickness and spacing, based on structural geometry assumptions, e.g. parallel plate model (Hildebrand & Ruegsegger, 1997a). However, using 3D images, such assumptions can be avoided, allowing the achievement of new model-independent quantitative parameters (Hildebrand & Ruegsegger, 1997b). Other methods, e.g. star volume distribution and star length distribution and applications of synchrotron

and conventional CT have been reviewed in (Wellington & Vinegar, 1987; Bonse & Busch, 1999; Ketcham & Carlson, 2001).

3. Synchrotron radiation microtomography for the *ex-vivo* and *in-vivo* evaluation of nanoparticle-labelled stem cell homing in muscular tissue

In recent works (Torrente et al., 2004; Gavina et al., 2006) it was shown that, after intra-arterial delivery to murine dystrophic muscle, human blood-derived CD133+ cells localize under the basal lamina and express the satellite cells markers M-cadherin and Myf5, differentiating into human muscle fibers and causing a significant amelioration of skeletal muscle structure.

The elucidation of the mechanisms involved in muscle homing of stem cells can aid in improving a potential therapy for muscular dystrophy based on the systemic delivery of such stem cells.

Combining nanoparticle cell labelling (A.K.Gupta & M.Gupta, 2005; Reimer & Weissleder, 1996) and X-ray synchrotron radiation micro-CT it is possible to provide detailed information on the stem cell migration in 3D, which are not attainable by traditional methods based on 2D techniques. In particular, micro-CT can give a relative local snapshot of the nanoparticle distribution (Brunke et al., 2005), with high spatial resolution images (from 10 μm to 1 μm) and high signal-to-noise ratio (Peyrin et al., 1998; Salomé et al., 1999).

Synchrotron radiation microtomography can be used for investigating the capacity of human stem cells to repair muscle damage in Duchenne Muscular Dystrophy.

In a first step, human blood-derived CD133+ cells were isolated from mononucleated cells collected by centrifugation (Ficoll-Hypaque; Pharmacia Biotech, Uppsala, Sweden) of several buffy coats, diluted 1:2 in RPMI 1640 medium (GIBCO, Invitrogen Life Technologies), incubated with CD133-phycoerythrin (CD133PE Miltenyi Biotech, Bergisch-Gladbach, Germany), and sorted to obtain purified CD133+ cells.

Stem cells were labelled with 250 μg/ml iron-oxide nanoparticles (Endorem) (Villa et al., 2010). Endorem is a magnetic contrast agent, based on dextran-coated Fe_3O_4 nanoparticles, with an average size of 150 nm. Labelling was performed in RPMI 1640 medium enriched with 20 ng/ml epidermal growth factor (EGF) and 10 ng/ml basic fibroblastic growth factor (bFGF) for 24 h. The average iron oxide content was 177 pg /cell.

The labelled CD133+ cells were injected into the femoral artery of scid/mdx mice. Different stem cell numbers ($5x10^4$, $1x10^5$ and $5x10^5$) were considered, at different times (0, 2, 12 and 24 h) after injection.

Ex-vivo and *in-vivo* measurements were carried out at the BM05 and ID19 beamlines, respectively, of the European Synchrotron Radiation Facility (ESRF) in Grenoble – France.

For the *ex-vivo* experiment, at different times (up to 24 hours) after cell transplantation *Tibialis Anterior* (TA) biopsies (2x2x2 mm^3) were isolated from injected legs to be studied by μ-CT (Torrente et al., 2006).

The optimal conditions for the X-ray absorption contrast among the different phases contained in the samples under investigation was obtained by varying the X-ray energy values between 18 and 27 keV. 1000 projections were recorded from each sample over 180°, with an exposure time of 1 s per projection. The detection system (2048x2048 FreLoN CCD camera) and the associated optics gave a pixel size of 1.65 μm, giving a field of view of about 3.3 x 3.3 x 3.3 mm^3. TA biopsies (2x2x2 mm^3) were isolated from injected legs and analyzed, for different numbers of initially injected cells ($5x10^5$, $1x10^5$ and $5x10^4$), as well as

different times after the injection (2, 12 and 24 h). In the *in-vivo* experiment, the living animals were anesthetized and the thigh region (about 7.5 mm height in total) of their left leg was exposed to the X-ray beam. X-ray beam energy was set to 24 keV; the pixel size was fixed at 7.5 μm, thus resulting in a field-of-view of 14.4 x 14.4 x 7.2 mm^3 (2048 x 2048 x 1024 voxels); 700 projections were collected with an acquisition time of 0.2 s/projection, giving a total radiation dose on the mouse of 40 - 45 Gy. Tomograms of the thigh region taken at 0 (actually approx. 10 min.), 2, 13 and 24 hours after injection were taken, in 3 different consecutive regions-of-interest (ROI) along the direction "parallel" to the femur, for a total thickness of 5.4 mm.

3.1 *Ex-vivo* experiments

The labelled cells are visualized as red spots in the reconstructed 3D volumes (Figure 1). A more accurate observation of the spatial distribution of the particles can be obtained by "deleting" the other phases by software (Figure 2).

The signal of labelled cells was clear at all concentrations greater than $5x10^4$ cells. No difference in the location of stem cells was observed at different times after injection, and stem cells appear to be distributed along the vessels.

The volume fraction of migrated labelled stem cells was calculated by counting their corresponding pixels (Figure 3).

In order to make sure that the Endorem signal is actually associated to the labelled CD133+ stem cells, muscle biopsies from mice injected with unlabelled cells and with "naked" Endorem nanoparticles were analyzed. No detectable signal was found in muscles injected with unlabelled CD133+ cells, as well as no Endorem nanoparticles were observed within the skeletal muscle after intra-arterial injection.

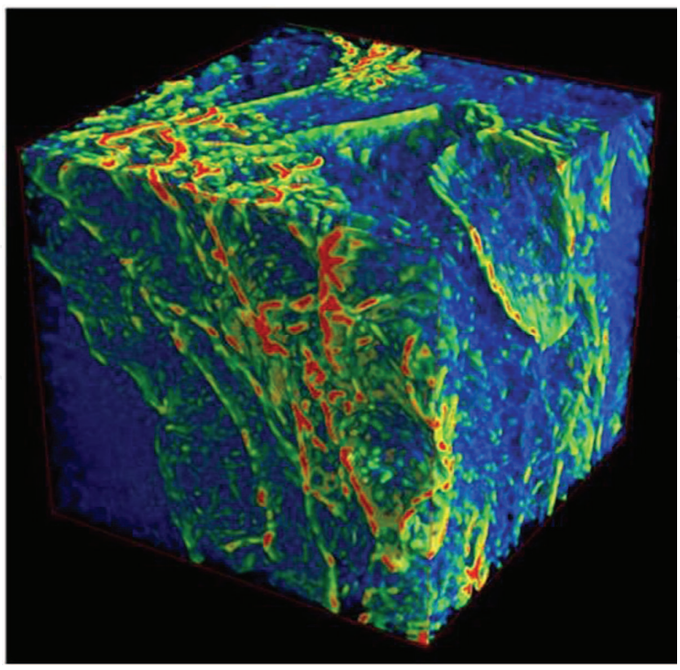

Fig. 1. 3D display showing the distribution of labelled stem cells ($5x10^5$ injected cells, 24 h after injection; red: labelled cells, green: vessels, blue: muscular tissue).

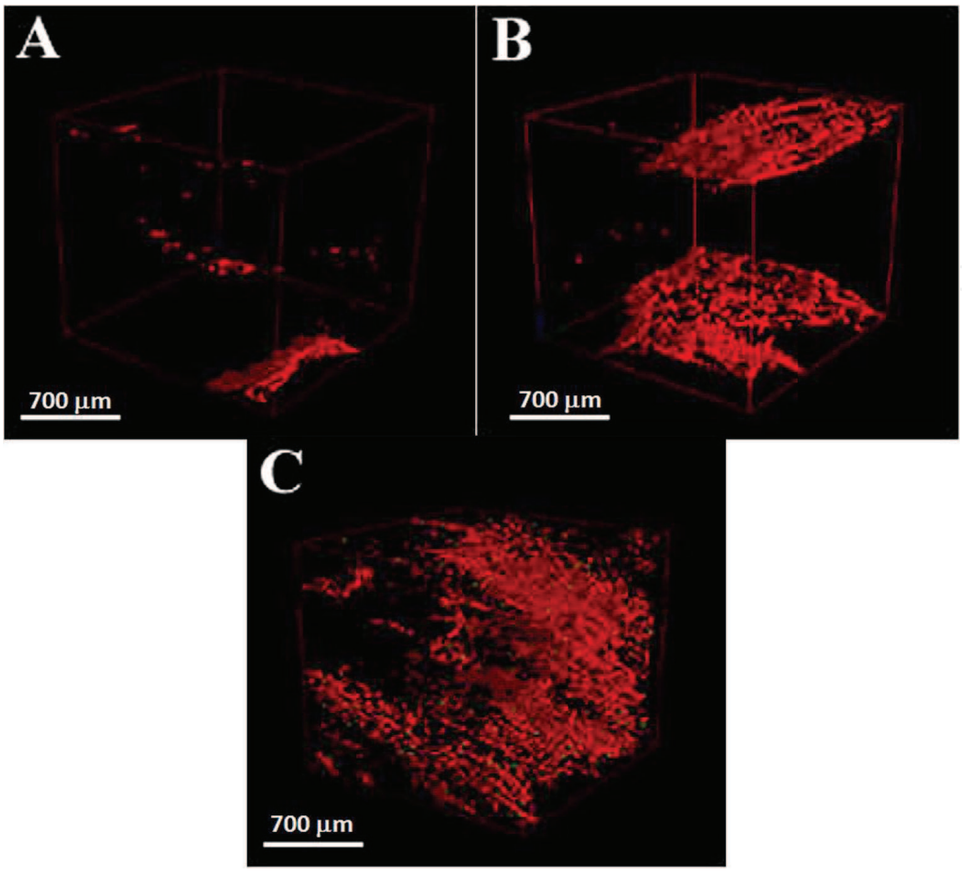

Fig. 2. 3D distribution of labelled stem cells (in red) within the muscle biopsies, 12 h after injection; A) $5x10^4$, B) $1x10^5$, C) $5x10^5$ injected cells.

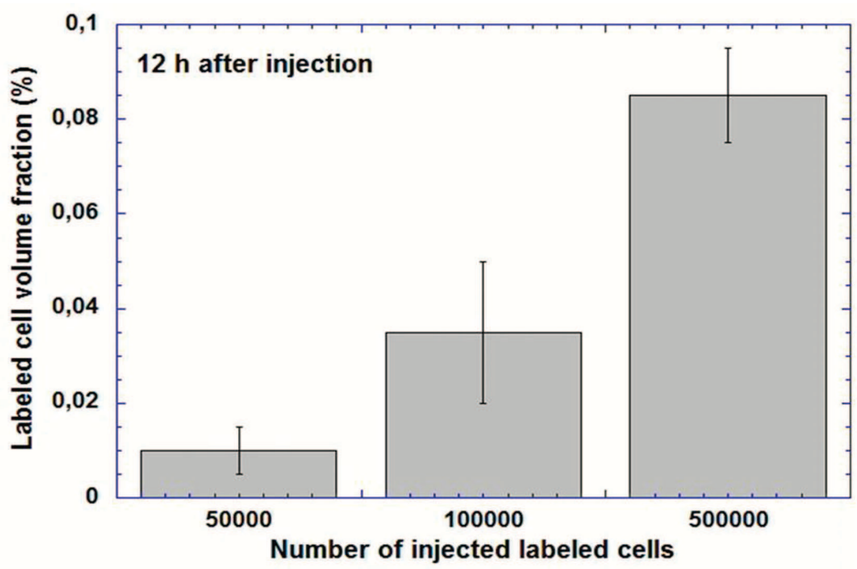

Fig. 3. Volume fraction of labelled cells in the muscle biopsies, 12 h after injection.

3.2 *In-vivo* experiments

The kinetics of the migration of stem cells into the muscular tissue was followed in the living mice, after injection of $5x10^5$ cells. To this end, one should notice that: i) μ-CT can reconstruct only objects that stay in place during the data acquisition, so that the signal coming from Endorem-labelled cells can only be due to cells that have actually migrated into the tissue, and not to those remained in the blood stream inside the vessels; ii) the small movements of the anesthetized animals, essentially due to their heartbeat (~ 10 Hz), induces two oscillations of the tissue during the acquisition time of each projection (0.2 s). Therefore the beam "sees" an apparent size of the cell as big as twice the oscillation amplitude; on this basis, assuming an oscillation amplitude of 200-300 μm, a factor ~ 50 in the apparent (measured) volume fraction with respect to the real one can be estimated.
Anyway, even though on a relative scale, the evaluation of the time evolution of this parameter is very important for the understanding of the migration kinetics.
Figure 4 shows the 3D distribution of the labelled stem cells in the investigated ROI (thigh region), for different times after injection.

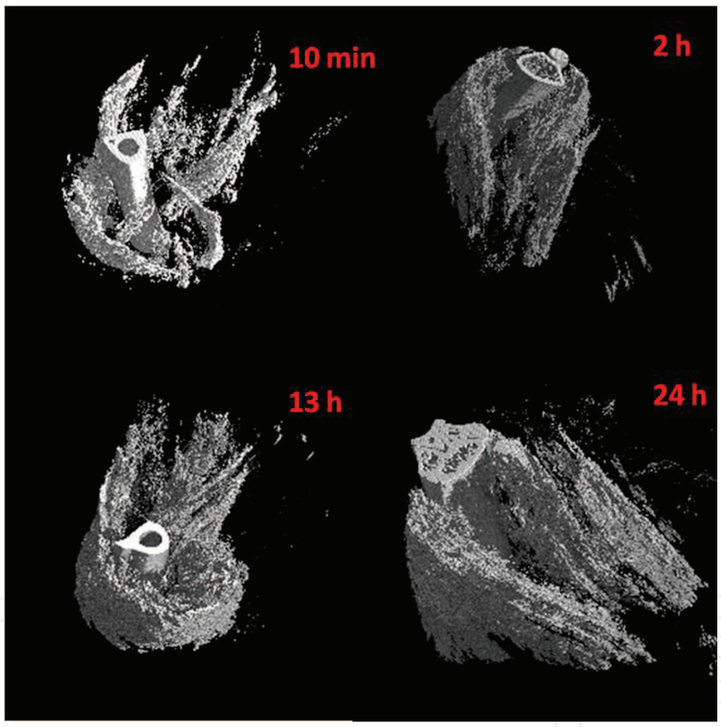

Fig. 4. 3D distribution of labelled stem cells in the femur region of the living mice, at different times after injection of $5x10^5$ cells.

In order to put into evidence the stem cells only, other tissues were eliminated by software in the image; anyway the femur bone could not be cancelled, as its absorption coefficient is similar to the Endorem one and the two corresponding peaks in the grey level histogram are superimposed. Therefore, the calculation of the apparent (in the sense described above) volume fraction of the stem cells was performed excluding the thigh region where the femur is present. The result for the calculated apparent volume fraction are shown in Figure 5, in which the most important feature evidenced is that the volume fraction is saturated after 2h.

In other words, the migration of the stem cells from the blood vessels to the muscular tissue happens within the first two hours from the injection. Synchrotron radiation micro-CT proved to be a powerful tool for the investigation of the labelled stem cells migration within the muscular tissue.

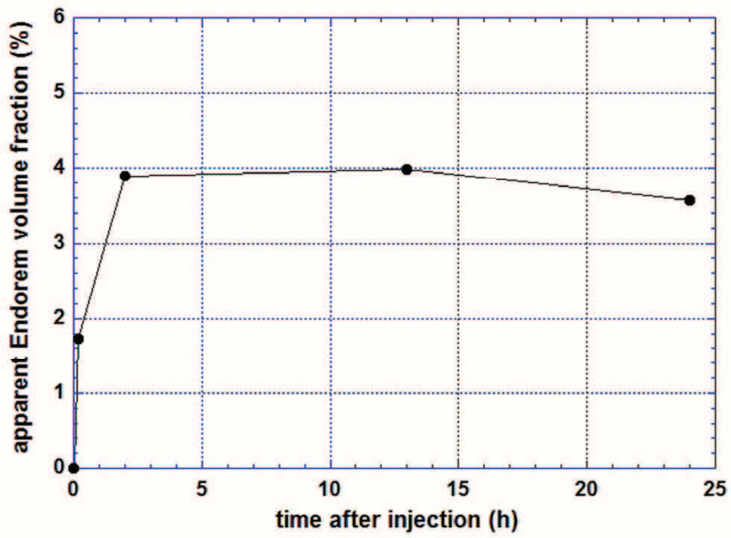

Fig. 5. Time evolution of the apparent volume fraction of labelled stem cells migrated into the muscular tissue, after injection of $5x10^5$ cells.

4. High-resolution X-ray microtomography for 3D imaging of cardiac progenitor cell homing in infarcted rat hearts

Experimental and clinical observations on the plasticity of adult stem cells has provided new tools in understanding the pathophysiology of cardiac diseases opening new strategies for the treatment of heart failure. Recent published reports (Leri et al., 2008; Kajstura et al., 2008; et al., 2006; Wollert et al., 2004; Balsam et al., 2004) have contributed to identify the possible approaches of cellular therapy to generate new myocardium, involving systemic and local mobilization of progenitor cells. Moreover, different laboratories (Beltrami et al., 2003; Oyama et al., 2007; Barile et al., 2007; Matsuura et al., 2004; Bearzi et al. 2007) have recently made available the unequivocal documentation of the existence, in the adult murine and human heart, of primitive cells able to generate all the different component structures of the myocardium. The possibility to rebuild muscle, arteries and capillaries is the necessary requirement to obtain successful approaches in cardiac regeneration, especially when taking into account the evidence that formation or implantation of a single cellular component will inevitably fail to repair the damaged organ (Menasche et al., 2008).

At tissue level of organization, microscopy techniques attempting to visualize the tissue rebuilding process, such as light, fluorescence, scanning and transmission electron microscopy are limited to two-dimensional (2D) local information or, otherwise, require laborious three-dimensional (3D) reconstruction of serial sections.

In-vivo imaging methods, including MRI, PET and micro-CT, have the potential to play a major role in the setting attempting to allow quantification of the rebuilding process, including longitudinal cell tracking (Badea et al., 2006; De Vries et al., 2005; Dhodapkar et

al., 2001; Schambach et al., 2010). On the other hand, current radiologic 3D-methods, possess intrinsic limitations to identify the localization and fate of the injected cells in both clinical (Frangioni & Hajjar , 2004) and experimental (Li et al.,2009; Toyama et al., 2004; Kudo et al., 2002; Schelbert et al., 2003) settings. All these contentions related to cell tracking methodologies for myocardial regeneration have been elegantly described (Terrovitis et al., 2010). Furthermore, a recent published report (Badea et al., 2006) comparing two imaging methods - namely MRM and micro-CT - for in-vivo preclinical studies on rodents, argued that both techniques require scan times that are much longer than a single respiratory or cardiac cycle. Real time imaging is not possible with the current state-of-the-art, unless active control of ventilation – that requires complex intubation of the animal – is performed. These serious limitations related to the observation of a beating heart (existing also in the other mentioned in-vivo experiments involving other imaging techniques), do not exist in the present work, which allows the visualization in 3D and at high-resolution (10-50 times higher than MRI) of the injected cells, with the possibility to quantify them and observe their fate within the myocardium one week after the injection.

In a recent study (Giuliani et al., 2010) it is explored the use of micro-CT as an experimental technique with high spatial resolution for detection of rat Cardiac Progenitor Cells (CPCs), previously labelled with iron oxide nanoparticles, inside the infarcted rat heart, one week after injection and in ex-vivo conditions. This work contributes to understand how and to which extent the injected cells are able to migrate and regenerate the damaged myocardium. This technique was demonstrated to offer the possibility of obtaining a 3D visualization of the cell spatial distribution and a quantification of the number of cells that are able to migrate from the site of injection to different areas of the rat heart tissue, with special reference to the infarcted myocardium. Importantly, to assess the validity of this approach, two additional independent methodologies of cell tracking, Quantum Dots labelling and genetically engineered EGFP cells, were applied.

The study population consisted of male Wistar rats (Rattus norvegicus) breed in the animal facility of the University of Parma - Dept. of Pathology, age 12-14 wk, weighing 350 - 400 g. An additional group of enhanced-Green Fluorescent Protein (GFP) transgenic rats were employed and kindly provided by Dr Okabe (Okabe et al., 1997).

Myocardial infarction was produced in rats and three weeks later implantation of 5×10^5 rat clonogenic CPCs (MI-FeCell group) was performed. Cells were labelled with Feridex Nanoparticles and supplemented with Hepatocyte Growth Factor (HGF, PeproTech EC, London, UK) and Insulin-Like Growth Factor-1 (IGF-1, PeproTech EC). Two animals were treated with implantation of equal number of Quantum Dots labelled (MI-QDot group) CPCs and two additional wild type animals with green fluorescence positive (GFP^{pos})-CPCs isolated from EGFP transgenic rats, both supplemented with HGF and IGF-1. One week later animals were sacrificed and the hearts were perfusion-fixed for analysis.

CPCs and GFP^{pos}-CPCs were obtained from 3 month old Wistar rats or enhanced-Green Fluorescent Protein (GFP) rat hearts, respectively, by Langhendorff perfusion apparatus as described in (Beltrami et al., 2003) with minor modifications. The solution containing all cells was washed several times, centrifuged at 300 rpm to remove cardiomyocytes and then submitted to Percoll (Sigma, Italy) gradient to further enrich the fraction of small cells. The cell layer visualized at the interface of the desired gradient was centrifuged at 1000 rpm and cells re-suspended in 10 ml of culture medium containing Iscove Modified Dulbecco's Medium (IMDM, Sigma, Italy) supplemented with 1% Penicillin-Streptomycin (P/S, Sigma, Italy), 1% Insulin-Transferrin-Sodium Selenite (I/T/S, Sigma, Italy), 10% Fetal Bovine Serum

(FBS, Sigma, Italy) and 10 ng/ml Basic-Fibroblast Growth Factor (b-FGF, Sigma, Italy) and seeded in Petri dishes (Corning, USA) placed at 37°C-5% CO_2 for their amplification.
Microscopic observation of cultures showed the growth of two different adherent cell populations, one with mesenchymal-like and one with monomorphic blast-like characteristics. This latter population constituted the so-called Cardiac Progenitor Cells (CPCs) provided by clonogenic growth and multipotency (Beltrami et al., 2003). These cells were amplified for several passages and cryopreserved in aliquots in a medium composed by FBS supplemented with 1% Dimethylsulphoxide (DMSO, Sigma, Italy) when needed for our experimental plan.
To detect homing and engraftment of the injected cells into murine hearts, CPCs were processed using the following protocols before their injection.
Before injection CPCs were loaded with super paramagnetic iron oxide nanoparticles (Feridex -Poly-L-Lysine (PLL) complex composed of 25μgFe/ml + PLL 375 ng/ml) for 24 hours. Then, medium was removed, CPCs washed with phosphate buffered saline (PBS) and trypsinized to be injected. Furthermore, Qtracker® 585 Cell Labelling Kit (QDots, Invitrogen, Italia) were employed, possessing an emission at 585 nm wavelength able to show QDots in yellow fluorescence after UV lamp excitation.
CPCs were stained with Qtracker® 585 Cell Labelling Kit which uses a custom targeting peptide to deliver yellow-fluorescent QDot® 585 nanocrystals into the cytoplasm of living cells. The protocol was performed following manufacture's suggestions.
In order to verify the efficiency of cell labelling, immediately before injection an aliquot of CPC suspensions was analysed under a fluorescence microscope equipped with UV lamp.
A micro-CT system (Beamline BM05 at the European Synchrotron Radiation Facility – ESRF Grenoble, France) was used to non-destructively image and quantify the 3Dmicrostructural morphology of each rat heart. The micro-CT experiment was performed in two modes: with a 15keV monochromatic X-ray beam and a sample-to-detector distance of 25 mm for the absorption-contrast and 500 mm for the phase-contrast, respectively. The acquisition setup was based on previously described (Torrente et al., 2006; Salome et al., 1999) 3D parallel tomography. 1500 projections and a step of 0.12 degrees were considered for each sample, with an exposure time of 1 s per projection.
3D reconstructions of the samples were obtained from the two series of 2D projections (for each sample one in absorption and the other one in phase-contrast configuration) using a 3D filtered back projection algorithm implemented at ESRF. The different phases found in the histogram referring to the reconstruction of the in-absorption acquisitions were coloured using a 3D display software in order to make them more easily recognizable. Furthermore, as the acquisitions were performed simultaneously, the combining absorption and phase contrast images did not required their geometric warping so that the corresponding image is structured correctly. Therefore, synchronization may be interactive or partially or fully automatic with help of a fusion algorithm which is described elsewhere (Stokking et al., 2003). The full fusion automatic algorithm was used. This exact synchronization of data sets provides capacity for image fusion with superimposition of both sets of imaging data in one image data set for further 3D visualization.

4.1 Fluorescence analysis

Once inside the cells, Qtracker® label provide intense, stable fluorescence that can be traced through several generations. QDots are not transferred to adjacent cells in a population of growing cells, enabling long-term studies of live cells and tissues.

CPCs pre-loaded with 585 QDots, were implanted by 3 injections in the peri-infarct region of the left ventricular wall of chronically infarcted heart. After heart excision, tissue sections of LV, RV and S were analyzed under UV-light and the fluorescence intensity of the QDots positive areas were analysed in photomicrographs covering the entire heart (Figure 6, A-B).

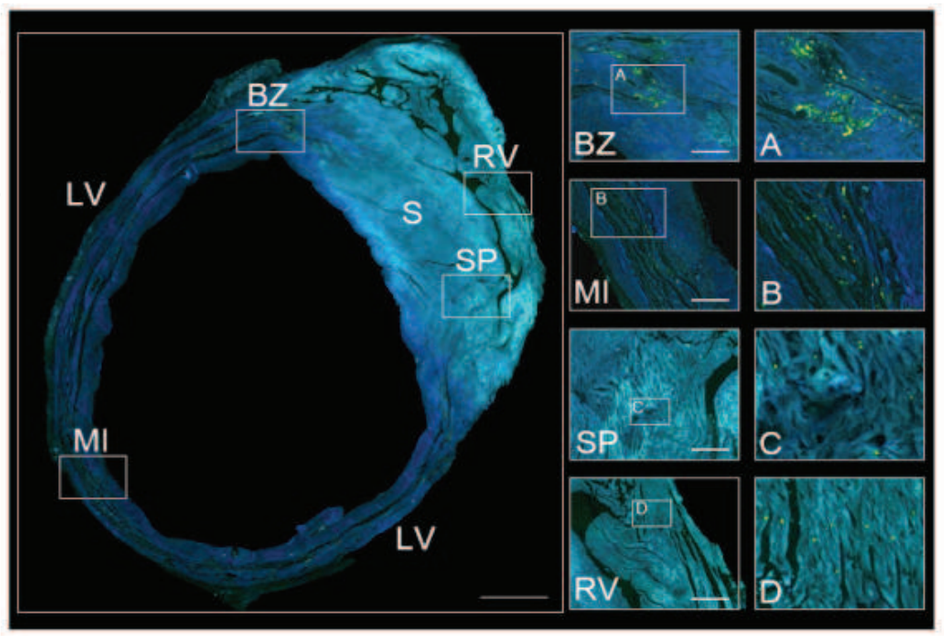

Fig. 6. Transverse section of a paraffin-embedded infarcted heart injected with CPCs and analyzed under UV-light to document the distribution of QDot labelled CPCs. Scale bars correspond to 1 mm in the left panels and to 200 μm in the right ones.

The results showed that CPC-related QDot signal was found in all regions of the heart although with different distribution and intensity. QDot-fluorescence was high and uniformly distributed in the infarcted (MI) and peri-infarcted (BZ) regions, from the site of injection following the total extension of the scar.
QDots were also occasionally found at very low occurrence in the spared myocardium (SP) and in the right ventricle (RV), far from the infarcted area and from the injection site.
To ascertain whether QDots signals were associated to living cells and not to nanoparticles released from death cells and uptaken by macrophages, the presence of GFP^{pos} cells in hearts injected with CPCs from EGFP transgenic rats was assessed. Immunofluorescence analysis showed that the distribution of GFP^{pos} cells present in the infarcted and spared myocardium one week after injection of GFP^{pos} CPCs, was similar to that observed in MI-QDots group. Interestingly, $GFP^{pos}/\alpha\text{-}Sarc^{pos}$ myocytes constituted ~15% of these cells and reached an average volume of 980±125 μm^3. The average cell volume of the remaining ~85% of GFP^{pos} cells found in the myocardium was 455 ± 76 μm^3.

4.2 Micro-CT analysis

The micro-CT analysis was used to non-destructively image and characterize, in absorption and in phase-contrast configuration, the 3D distribution of the rat CPCs one week after their injection into an infarcted rat heart. Two biopsies of infarcted rat hearts, both injected with

$5 \cdot 10^5$ stem cells labelled by iron-oxide nanoparticles, 1 week after injection were analyzed. The harvested heart samples were scanned and projection data were obtained and reconstructed into 2D images. A portion of a reconstructed 2D slice is shown in Figure 7 (A). The basic physical parameter quantified in each pixel of an absorption micro-CT image and exploited to obtain the contrast is the linear X-ray attenuation coefficient μ. The X-ray attenuation produced by the Feridex-positive stem cells is higher than attenuation referred to the other tissues of the injected hearts, allowing their visualization as bright spots in the 2D images (magenta coloured spots in Figure 7 (A)). The differences in the X-rays absorption rate within the samples translate into different peaks in the grey level scale corresponding to the different phases. The histogram of the grey level scale is shown in Figure 7 (B) and 7 (C). The volume of each phase is obtained by multiplying the volume of a voxel (~125 μm^3) by the number of voxels underlying the peak associated with the specific phase. The volume percentage of the CPCs respect to the total investigated volumes is very low (as shown in Table 1), as expected by considering the amount of the injected CPCs: for this reason the peak corresponding to the labelled CPC phase is not visible in Figure 7 (B) but can be easily detected in the inset (Figure 7 (C)), magnifying the respective portion of the histogram.

The slice images were compiled and analysed to render 3D images and to obtain a better visualization of the stem cell distribution after their injection in the infarcted rat hearts. Regions of interest were selected in each slice image and thresholded to eliminate background noise. The thresholded 3D volumes were converted into coloured images using a 3D display software, by means it is possible to correlate the bright spots of labelled cells present in the 2D images (Figure 7 (A)) with the spots distributed in the 3D reconstruction (Figure 8 (C) and (D)).

3D display of fusion images is represented on Figure 8. In combined imaging, morphological information about heart tissue from phase contrast is complemented and extended by the functional information on labelled-CPCs supplied from absorption mode.

Furthermore, the simple segmentation process provides information on the internal structure of the heart (Figure 8 (B)) and the distribution of the CPCs within it (Figure 8 (C) and (D)). Subsequently, different 3D sub-regions of interest with detailed information are illustrated in Figure 8 (E) and (F).

No dramatic difference in the location of stem cells was observed in the two hearts: the percentage of migrated labelled stem cells from the injection area to the infarcted area or towards other areas was calculated by counting their corresponding pixels, using the algorithm that automatically separates them from the other tissues. The obtained data were expressed as percentage of the analysed sample volume and are listed in Table 1.

The micro-CT was used to image and characterize the 3D spatial distribution of injected rat clonogenic cells (CPCs) inside the heart tissue of infarcted mice after cell labelling by iron oxide nanoparticles.

The 3D visualization of the spatial distribution of the grafted cells with respect to myocardium and vascular system was obtained. In particular, the X-ray absorption of the labelled cells was higher than that of host tissues, allowing their visualization as bright spots in the 2D images (Figure 7).

These slice images were compiled and analyzed to render 3D images and to obtain a better visualization of cell distribution within the samples (Figure 8). One week after injection, labelled cells were distributed mostly in proximity and towards the damaged infarcted area

(Figure 8 (F)), demonstrating migration of CPCs from the injection site made around the coronary binding. It was also possible to identify finger-like cell structures in the inner part of the left ventricular wall (Figure 8 (D) and Figure 8 (F)).
It was also observed single smaller units, in all areas of the heart, as in the atria, in large vessels (Figure 8 (E)) and in the right ventricle. These are very important and new data: in particular they constitute a confirmation that these cells can migrate through the myocardium by a biological mechanism which is still unknown.

	Total Volume of the investigated rat heart [μm³]	**Total Volume V_{tot} of CPCs* [μm³]**	**Infarcted Area (%)**	**Perinfarcted Area (%)**	**Remaining Area (%)**	**CPC Volume Fraction (%)**	**Total CPC number *N***
Sample I	**321676 ·10⁶**	**595 ·10⁶**	**77.9**	**4.3**	**17.8**	**0.18**	**~ 1.11X10⁶**
Sample II	**331265 ·10⁶**	**995 ·10⁶**	**97.8**	**1.6**	**0.6**	**0.30**	**~ 1.86X10⁶**

* Total Volume filled by the CPCs [μm³]

Table 1. Quantitative Parameters obtained in absorption configuration.

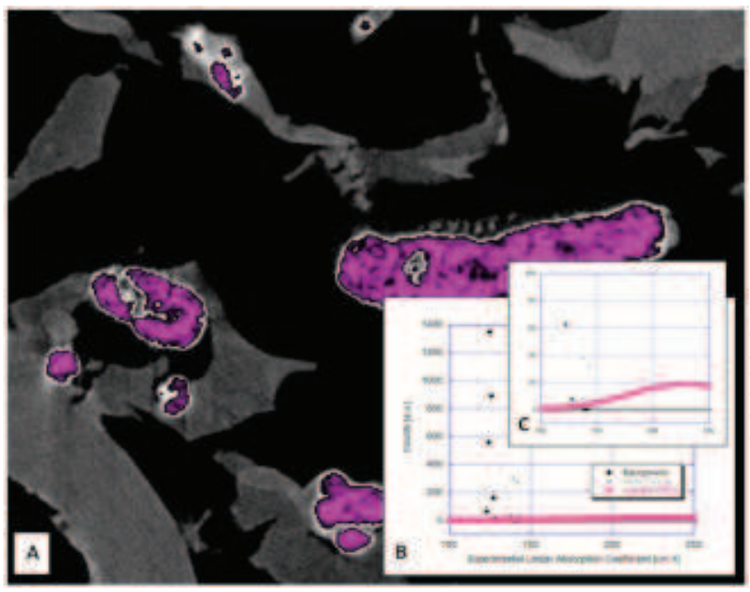

Fig. 7. (A) Portion of a reconstructed 2D slice. The X-ray attenuation produced by the labelled cells is higher than attenuation referred to the other tissues of the injected hearts, allowing their visualization as bright spots in the 2D images (magenta coloured spots). (B) The histogram of the grey level scale corresponding to the different detected phases. (C) Magnification of the portion of the histogram shown in B referred to the peak corresponding to the labelled cells grey level.

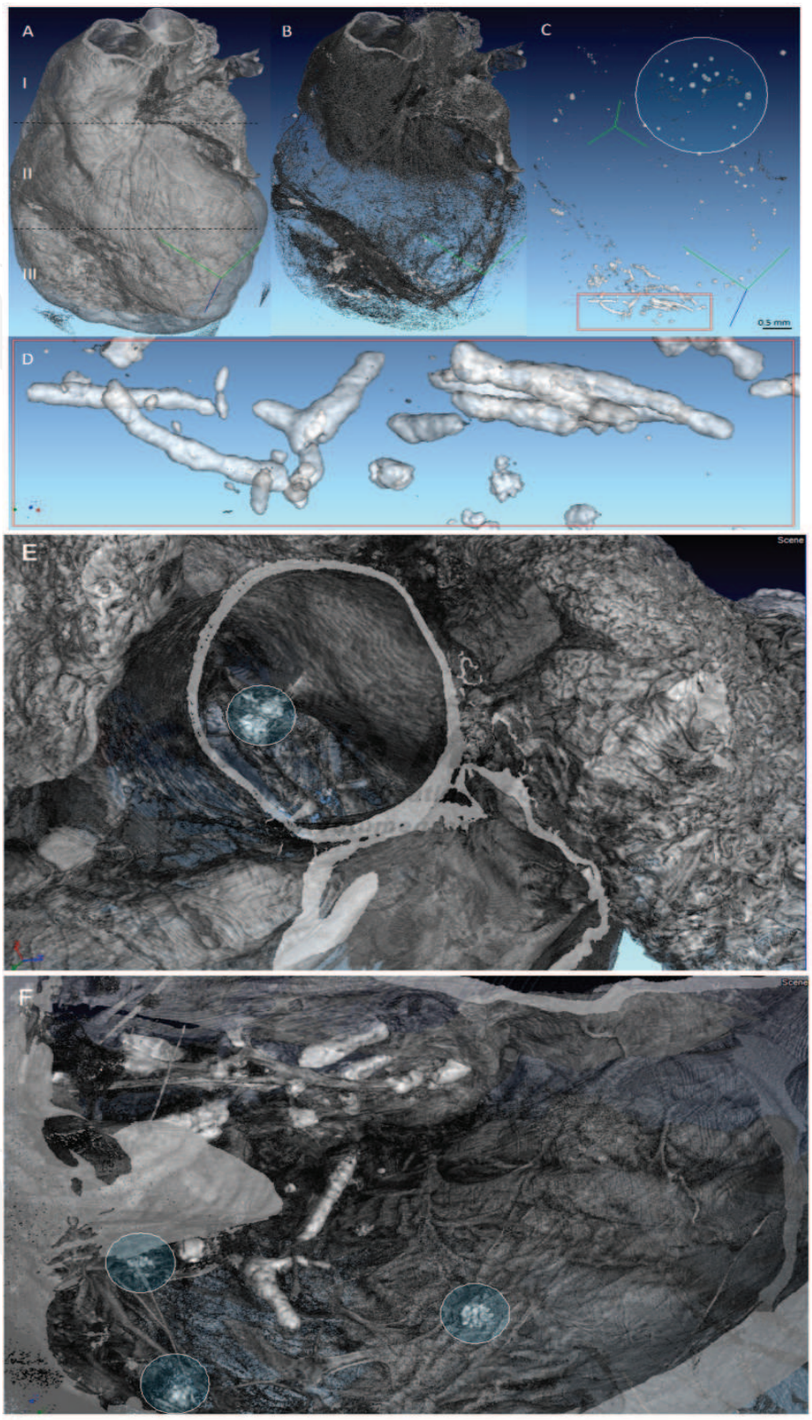

Fig. 8. (A) 3D display of fusion images. The simple segmentation process provides information on the internal structure of the heart (B) and the distribution of labelled cells (C) and (D). Fusion images of two different 3D sub regions of interest: (E) - atria and large vessels; (F) - infarcted area. Individual cells and small cell clusters are pointed out in the lighted circles.

Importantly, results obtained by micro-CT were in close agreement with imaging of the distribution of QDots, strongly suggesting the validity of these methodologies to detect cell engraftment within the damaged heart.
The issue whether either iron particles, as detected here by micro-CT, or QDots nanoparticles, as detetcted by UV excitation, could only represent unreliable signals of macrophages uptaking tracers released by dying cells, remains an unresolved problem especially on clinical ground. However, an effort was made by the present investigation to apply a third independent genetic marker to visualize the progeny of the injected cells. Thus, CPCs from rats carrying the EGFP transgene were employed and GFP labelled cells counted by immunofluorescence. This approach allowed us to ensure that the progeny of the injected cells was present in the infarcted heart and with a similar distribution to that observed with QDots labelling and micro-CT imaging. Importantly, not only survival but also differentiation of CPCs into cardiomyocytes was demonstrated by the presence of GFP positive cells with α-sarcomeric striation. Thus, whether unspecific signals were concomitantly detected by fluorescence or X ray cannot be excluded although with minimal impact on the overall results.
Indeed, it was estimated the total number N of the cells found in the hearts one week after CPC injection (as reported in Table 1). It was found out that in both hearts the number N of CPC-derived cells is more than doubled with respect to the number of injected CPCs, demonstrating that, at least for labelled CPCs and at a week from injection, the presence of Feridex does not dramatically affect the CPC life span.
In conclusion, the obtained 3D images represent a very innovative progress, as compared to the usual 2D histological images, which do not provide the overall 3D distribution of rat clonogenic cells and their progeny within the heart, providing biological insights into the early processes of cell migration.

5. Application of X-ray synchrotron radiation techniques to bone tissue engineering

Tissue engineering is a promising approach to create artificial constructs for repairing or replacing partially or entirely diseased tissues (Williams, 2004; Langer & Vacanti, 1993).
A key component in tissue engineering for bone regeneration is the scaffold, which acts as a template for cell interactions and for the growth of bone extracellular matrix to provide structural support for the newly formed tissue (Karageorgiou & Kaplan, 2005). Many researchers have tried to define which properties are required for the optimal synthetic scaffold, in particular for bone tissue replacement (Hutmacher, 2000).
Ideally, scaffolds should possess adequate mechanical strength and permeability (van Lenthe et al., 2007), high porosity (Shi et al., 2007), large surface area to volume ratio, as well as biocompatibility and non- toxicity (Murugan & Ramakrishna, 2006). Moreover, pore interconnectivity is an important scaffold criterion (Moore et al., 2004) which influences nutrient supply (Hui et al., 1996), circulation of extracellular material (Gross & Rodriguez-Lorenzo, 2004), the contact between adjacent cells (Darling & Sun, 2004), and the promotion of blood vessel and bone tissue ingrowth (Kuboki et al., 1998).
Commonly, two-dimensional (2D) investigation methods, such as scanning electron microscopy (SEM) are used for the characterization and comparison of the scaffolds. Unfortunately, these methods do not allow a complete investigation of the three dimensional (3D) spatial structure of the scaffold. More recently, micro-CT has been

proposed for the characterization of scaffolds and 3D bone ingrowth (Mastrogiacomo et al., 2004).

In the recent years, a lot of progress was obtained in the field of bone tissue engineering by using innovative analytical and diagnostic imaging techniques, such as micro-CT and pseudo-holotomography.

X-ray synchrotron microtomography was applied (Komlev et al., 2006) to investigate highly porous hydroxyapatite scaffolds, previously seeded with bone marrow stromal cells (BMSC), implanted in an immunodeficient murine model. It was proved that it was possible to obtain in a nondestructive way a quantitative analysis of tissue engineering constructs, determining the total volume and thickness distribution of newly formed bone into implants in a small animal model, by using the micro-CT technique. This methodology offers major advantages, including the possibility of investigating the influence of scaffold parameters, such as porosity and spatial distribution of the structure thickness, on the bone growth within the implant.

Very recently, different ceramic scaffolds with high porosity were characterized (Komlev et al., 2010) and it was evaluated the bone growth into the tissue engineering constructs *ex vivo* at different implantation times, by using synchrotron radiation micro-CT. In this study, three types of ceramic scaffolds with different composition and structure (namely synthetic 100% hydroxyapatite (HA; Engipore), synthetic calcium phosphate multiphase biomaterial containing 67% silicon stabilized tricalcium phosphate (Si-TCP; Skelite™) and natural bone mineral derived scaffolds (Bio-oss®), were seeded with mesenchymal stem cells (BMSC) and ectopically implanted for 8 and 16 weeks in immunodeficient mice. X-ray synchrotron radiation microtomography was used to derive 3D structural information on the same scaffolds, both before and after implantation. The images of the three scaffolds before implantation revealed an appreciable difference among their morphologies (Figure 9). In particular, the Bio-Oss®, contained elongated ellipsoidal pores, whereas the HA scaffold contained roughly spherical pores.

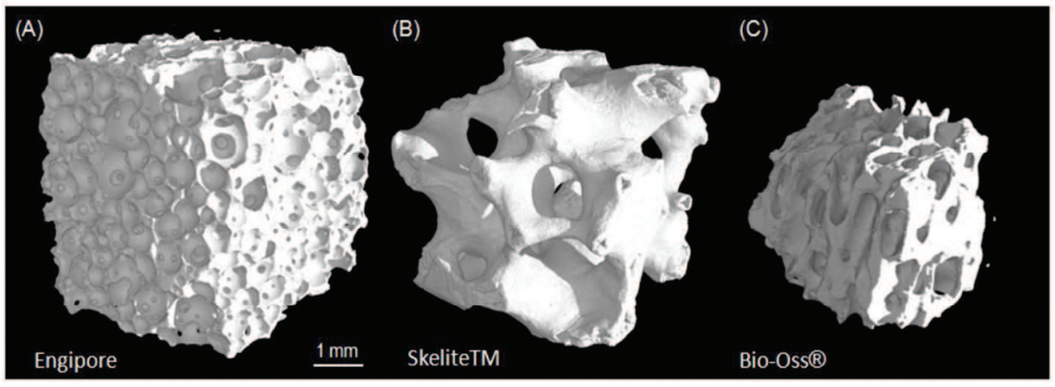

Fig. 9. 3D display of different scaffolds before implantation: **(A)** Engipore (hydroxyapatite) produced by FinCeramica, Faenza, Italy; **(B)** SkeliteTM (silicon-stabilized tricalcium phosphate) produced by Millenium Biologics Kingston, Ontario, Canada; **(C)** Bio-Oss® (natural bone mineral) produced by Geistlich Pharma AG, Wolhusen, Switzerland (Komlev et al., 2010).

Figure 10 (Panels A1-C1), obtained by an innovative imaging procedure, gives an instantaneous pictorial view of the wall thickness distribution in the scaffold and confirms

the results previously obtained in (Papadimitropoulos et al., 2007), namely biodegradation for the Si-TCP scaffold and lack of it for the HA scaffold. The newly investigated Bio-Oss® showed a very little decrease of the scaffold wall thickness; the decrease was at the limit of detectability, and needs to be confirmed by additional experiments.

Based on these findings, the scaffold biodegradation in the tissue engineered implanted constructs was investigated after 16 weeks implantation only for the Skelite™. 3D displays of registered images of pre- and post implantation Skelite™ samples implanted for 8 (A) and 16 (B) weeks are presented in Figure 11 (panels A-B). As it appears in the images in Figure 10 (panel B2), blue and yellow correspond to totally or partially resorbed scaffold. The volume percentage distribution of the different phases is presented in panels A1 and B1. An increase in the percentage of the resorbed scaffold was observed in the case of a longer implantation time.

The analysis proposed in the manuscript (Komlev et al., 2010) is, therefore, a major improvement as compared to the imaging procedure adopted in our previous work (Papadimitropoulos et al., 2007), where only a comparison between different subvolumes of the implants before and after implantation was made.

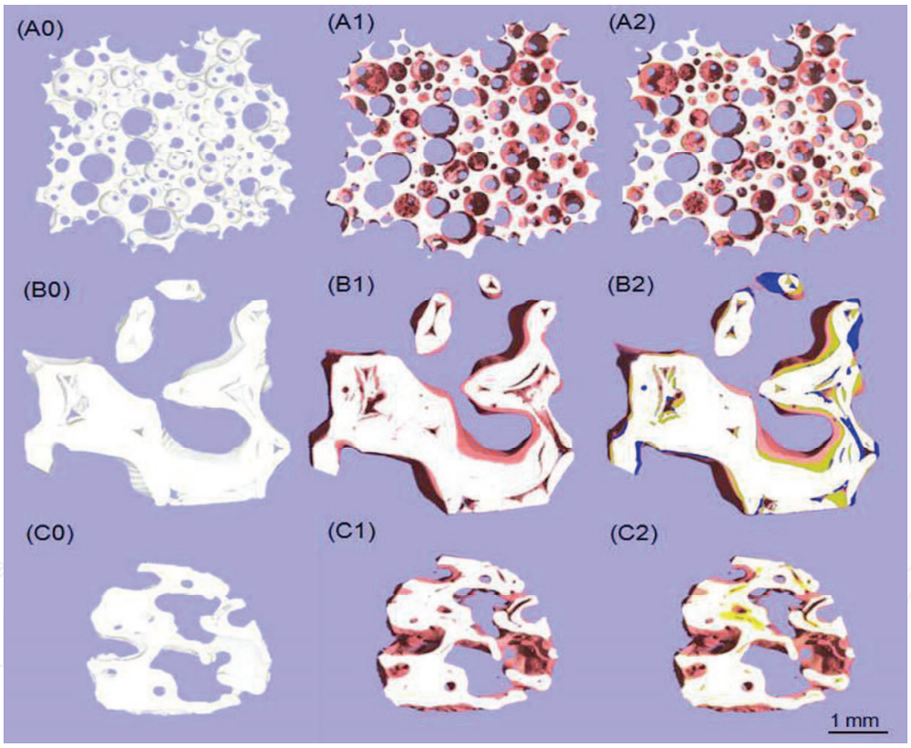

Fig. 10. 3D display of subvolumes of scaffolds before and after implantation: (A) Engipore; (B) SkeliteTM; (C) Bio-Oss®; (A1-C1). New bone (pink) on the surface of the scaffolds (white). In the panels A2-C2 are presented the images obtained by combining (registering) the data of panels A0-C0 with those of panels A1- C1. Blue volumes indicate portions of scaffolds present in panels A0-C0 (pre-implant) and absent in panels A1-C1 (after implantation) and correspond to completely resorbed scaffold. Yellow volumes indicate virgin scaffold volume in which after implantation a reduction of the sample density is observed (Komlev et al., 2010).

Finally, a high content of innovation is associated to the detailed kinetics studies on the Skelite™ scaffolds implanted for different times, not only due to the large number of the implantation times investigated, but also to the recording in the X-ray absorption histograms of separate peaks associated to HA and TCP in the same scaffold (Figure 12).
It is therefore possible to observe that the progressive biodegradation of Skelite™ scaffold is eventually due to the TCP component. It should be noted that when investigated by microdiffraction studies, the local structural study at the interface between the newly formed bone and the Skelite™ scaffold indicated that scaffold biodegradation was mainly due to TCP depletion (Papadimitropoulos et al., 2007).
Moreover, saturation in the TCP biodegradation occurred at an implantation time of about 10 weeks, whereas saturation in the tissue engineered bone occurred at an implantation time of about 22 weeks.
This could indicate that the bone growth did not occur only in the scaffold volume that was resorbed, but also in the inward direction with respect to the pore surface. This finding is in agreement with the results presented in Figure 5 of reference (Mastrogiacomo et al., 2007), and in Figure 4 of reference (Papadimitropoulos et al., 2007).

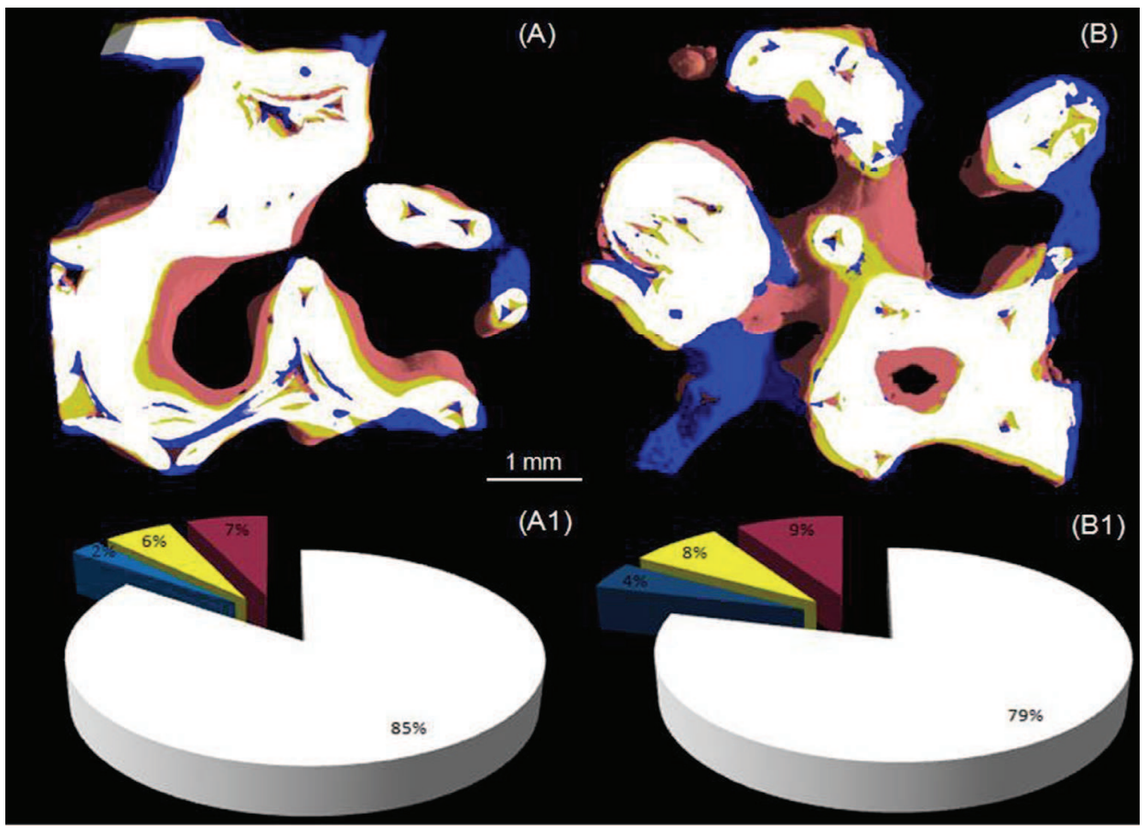

Fig. 11. Display based on a combination of the 3D structure of pre- and post implanted SkeliteTM samples for 8 (A) and 16 (B) weeks, respectively (white – scaffold; pink – new bone; blue – total resorption; yellow – partial resorption (see caption of Figure 10). (A1-B1) volume percentage distribution of the different phases (Komlev et al., 2010).

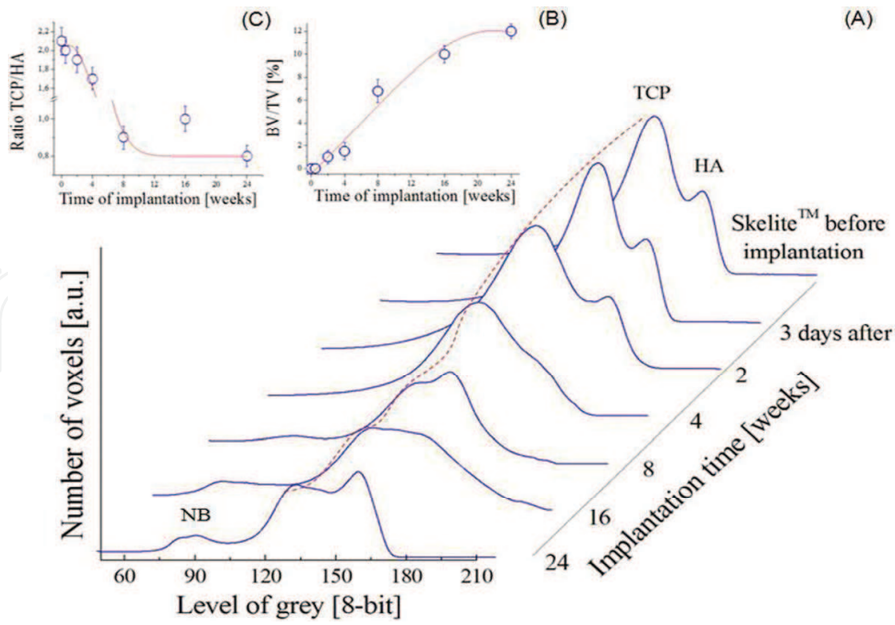

Fig. 12. Volume histograms of SkeliteTM scaffolds implanted from 3 days to 24 weeks (NB – new bone, TCP – tricalcium phosphate, HA – hydroxyapatite). (A) New bone deposition kinetics; (B) Percentage of bone volume/ total volume; (C) TCP/HA mean ratio as a function of the implantation time (Komlev et al., 2010).

Figure 13 (A) and (B) presents a 3D reconstruction of a bone tissue- engineered construct, 24 weeks after the implantation. Three phases are clearly distinguishable: the scaffold (white), the engineered bone (light brown), and the vessel networks within the pores (green). In Figure 13 (B), the engineered bone was removed by digital processing to obtain a clearer evidence of vessel network structure.

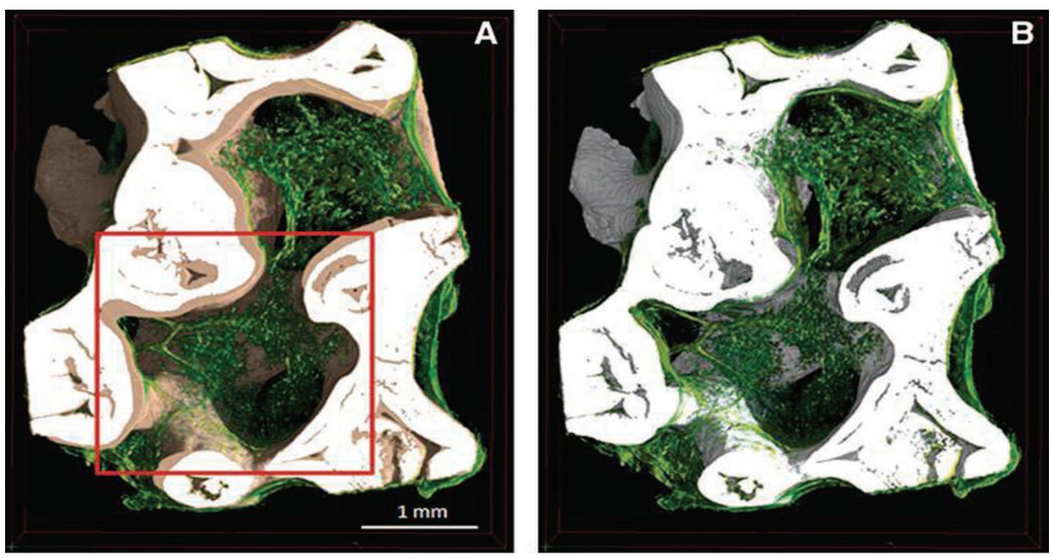

Fig. 13. 3D enhanced contrast micro-CT images of the tissue-engineered construct after 24 weeks of implantation in an immunocompromised mouse. (Komlev et al., 2009).

In absorption micro-CT, the image contrast results from the difference among different attenuation coefficients of X-ray for the different materials. Unfortunately, X-ray attenuation coefficients of soft tissues are low, and, thus, the contrast difference of these structures is low, unless a contrast agent is adopted. Therefore, in a recent study (Komlev et al., 2009), it was proposed to use X-ray synchrotron radiation pseudo-holotomography to visualize microvascular networks, at a three-dimensional (3D) level, for the first time with no need for contrast agents, and to extract quantitative structural data in a Bioceramic/MSC composite implanted for 24 weeks in a mouse.

The enhanced contrast micro-CT technique is a new imaging method based on classical micro-CT and recently developed technique of holotomography. By using a coherent X-ray beam, phase contrast may be simply obtained by free space propagation (i.e., by positioning the detector at some distance from the sample), while a 2D projection of the phase map can be obtained from three or four series of images, each series being recorded at different distance from the object for each rotation angles considered. Then, the 3D phase map is reconstructed with the same algorithm as in classical tomography (Cloetens, 2009). Anyway, through the weighted superposition of both attenuation and phase maps (enhance contrast micro-CT), it is possible to generate better images.

Vessels are easy to see also in 2D micro-CT images (Figure 14 (A)). Figure 14 (B) shows a histogram of the 3D vessel diameter distribution measured within the full volume of the sample implanted for 24 weeks. The mean vessel diameter measured from pseudo-holotomography data was 49±25 μm. This value was comparable to the 47±18 μm measured in control histology sections.

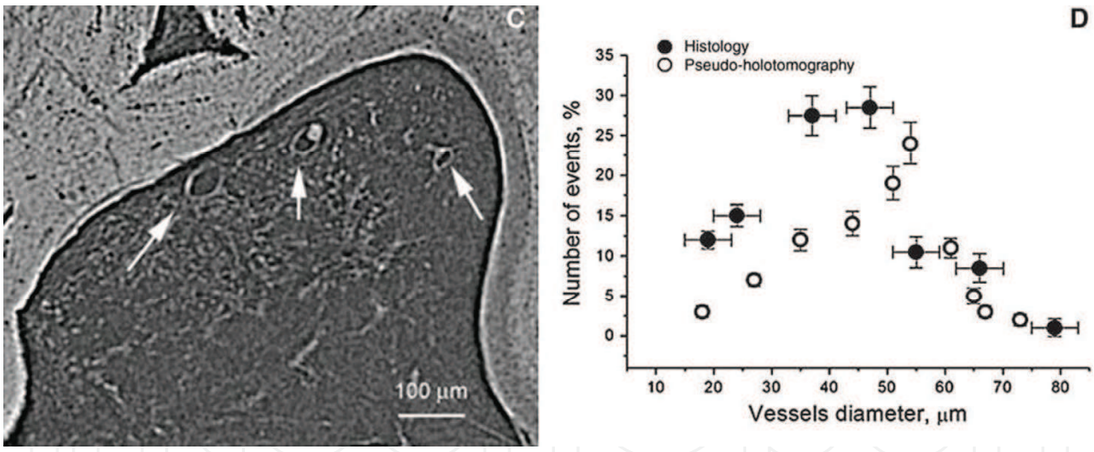

Fig. 14. 2D micro-CT image (A) and (B) histogram of the vessel diameter distribution measured for pseudo-holotomography data (open circle) and histology (solid circle) (Komlev et al., 2009).

This progress could be extrapolated to different biomedical research areas where angiogenesis and microvasculogenesis play an important role, as for the development of tissues such as bone, in regenerative medicine, or in pathologies characterized by inflammation and tissue damage such as diabetes, osteoarthritis, and muscular dystrophy. Of great interest could also be the application of the pseudo-holotomography to investigations of therapeutical roadmaps for tumor treatment involving the suppression of vascularization.

6. References

Arbab, A.S., Bashaw, L.A., Miller, B.R., Jordan, E.K., Bulte, J.W. & Frank, J.A., Intracytoplasmic tagging of cells with ferumoxides and transfection agent for cellular magnetic resonance imaging after cell transplantation: methods andtechniques. Transplantation 2003, 76: 1123.

Ashbridge, D.A., Thorne, M.S., Rivers, M.L., Muccino, J.C. & O'Day, P.A., Image optimization and analysis of synchrotron X-ray computed microtomography (CT) data, Computers & Geosciences 2003, 29: 823–36.

Atala, A. Tissue engineering, stem cells and cloning: current concepts and changing trends, Expert Opin Biol Ther. 2005, 5(7): 879-92.

Badea, C.T., Hedlund, L.W. & Johnson, G.A., Micro-CT with respiratory and cardiac gating, Med Phys., 2004, 31: 3324–3329.

Balsam, L.B., Wagers, A.J., Christensen, J.L., Kofidis, T., Weissman, I.L. & Robbins, R.C., Haematopoietic stem cells adopt mature haematopoietic fates in ischaemic myocardium. Nature,2004, 428:668 –73.

Barile, L., Chimenti, I., Gaetani, R., Forte, E., Miraldi, F. & Frati G., Cardiac stem cells: isolation, expansion and experimental use for myocardial regeneration. Nat Clin Pract Cardiovasc Med, 2007, 4 (Suppl 1):S9 –14.

Bearzi, C., Rota, M., Hosoda, T., Tillmanns, J., Nascimbene, A. & De Angelis, A., Human cardiac stem cells. Proc Natl Acad Sci USA, 2007, 104:14068 –73.

Beltrami, A.P., Barlucchi, L., Torella, D., Baker, M., Limana, F. & Chimenti, S., Adult cardiac stem cells are multipotent and support myocardial regeneration. Cell, 2007, 114:763–76.

Bonse, U. & Busch, F., X-ray computed microtomography (μCT) using synchrotron radiation (SR). Progr in Bioph and Molec Biol 1999; 65(1/2): 133–69.

Boskey, A. & Pleshko Camacho, N. FT-IR imaging of native and tissue-engineered bone and cartilage. Biomaterials 2007, 28: 2465.

Brunke, O., Odenbach, S., Fritsche, C., Hilger, I. & Kaiser, W.A., Determination of magnetic particle distribution in biomedical applications by X-ray microtomography, J. Magnet. Mag. Mater. 289 (2005) 428–430.

Bulte, J.W., Duncan, I.D. & Frank, J.A. In vivo magnetic resonance tracking of magnetically labelled cells after transplantation.J. Cereb. Blood Flow Metab. 2002, 22: 899.

Campbell, C.T. & Kim, G., SPR microscopy and its applications to high-throughput analyses of biomolecular binding events and their kinetics. Biomaterials 2007, 28: 2380.

Claesson, T., A medical imaging demonstrator of computed tomography and bone mineral densitometry. Stockholm: Universitetsservice US AB; 2001.

Cloetens, P., Holotomography: quantitative phase tomography with micrometer resolution using hard synchrotron radiation X rays. Appl Phys Lett, 2009, 75: 2912.

Darling, A.L. & Sun, W., 3D microtomographic characterization of precision extruded poly-epsilon-caprolactone scaffolds. Journal of Biomedical Materials Research Part B - Applied Biomaterials 2004, 70B (2):311–317.

De Vries, I.J.M., Lesterhuis, W.J., Barentsz, J.O., Verdijk, P., Van Krieken, J.H. & Boerman, O.C., Magnetic resonance tracking of dendritic cells in melanoma patients for monitoring of cellular therapy. Nature Biotechnology, 2005, 23: 1407 - 1413.

Dhodapkar, M.V., Steinman, R.M, Krasovsky, J., Munz, C. & Bhardwaj, N., Antigen-specific inhibition of effector T cell function in humans after injection of immature dendritic cells. J Exp Med, 2001, 193:233-8.

Eniwumide, J.O., Yuan, H., Cartmell, S.H., Meijer, C.J. & de Bruijn, J.D., Ectopic bone formation in bone marrow stem cell seeded calcium phosphate scaffolds as compared to autograft and (cell seeded) allograft. Eur. Cells Mater. 2007, 14: 30.

Frangioni, J.V. & Hajjar, R.J., In Vivo Tracking of Stem Cells for Clinical Trials in Cardiovascular Diseases. Circulation, 2004, 110:3378-3384.

Gavina, M., Belicchi, M., Rossi, B., Ottoboni, L., Colombo, F., Meregalli, M., Battistelli, M., Forzenigo, L., Biondetti, P., Pisati, F., Parolini, D., Farini, A., Issekutz, A.C., Bresolin, N., Rustichelli, F., Constantin, G. & Torrente, Y., VCAM-1 expression on dystrophic muscle vessels has a critical role in the recruitment of human blood-derived CD133+ stem cells after intra-arterial transplantation, Blood 108(8) (2006) 2857-2866.

Giuliani, A., Frati, C., Rossini, A., Komlev, V. S., Lagrasta, C., Savi, M., Cavalli, S., Gaetano, C., Quaini, F., Manescu, A. & Rustichelli, F. , High-resolution X-ray microtomography for three-dimensional imaging of cardiac progenitor cell homing in infarcted rat hearts. Journal of Tissue Engineering and Regenerative Medicine, n/a. doi: 10.1002/term.409

Gross, K.A. & Rodriguez-Lorenzo, L.M., Biodegradable composite scaffolds with an interconnected spherical network for bone tissue engineering. Biomaterials 2004, 25 (20):4955–4962.

Gupta, A.K. & Gupta, M., Synthesis and surface engineering of iron oxide nanoparticles for biomedical applications, Biomaterials 2005, 26: 3995–4021.

Hildebrand, T. & Ruegsegger, P., A new method for the model independent assessment of thickness in three-dimensional images. J Microsc, 1997; 185: 67–5.

Hildebrand, T. & Ruegsegger, P., Quantification of bone microarchitecture with the Structure Model Index. Comput Meth Biomech Biomed Engng 1997; 1: 15–23.

Hill, J.M., Dick, A.J., Raman, V.K., Thompson, R.B., Yu, Z.X. & Hinds, K.A. Serial Cardiac Magnetic Resonance Imaging of Injected Mesenchymal Stem Cells. Circulation 2003, 108: 1009.

Hoehn, M., Kustermann, E., Blunk, J., Wiedermann, D., Trapp, T., Wecker, S., Focking, M., Arnold, H., Hescheler, J., Fleischmann, B.K., Schwindt, W. & Buhrle, C. Monitoring of implanted stem cell migration in vivo: a highly resolved in vivo magnetic resonance imaging investigation of experimental stroke in rat. Proc Natl Acad Sci U S A. 2002; 99: 16267–16272.

Hui, P.W., Leung, P.C. & Sher, A. Fluid conductance of cancellous bone graft as a predictor for graft–host interface healing. Journal of Biomechanics 1996, 29 (1):123–132.

Hutmacher, D.W., Scaffolds in tissue engineering bone and cartilage. Biomaterials 2000,21:2529–43.

Jones, J.R. & Hench, L.L. Regeneration of Trabecular Bone using Porous Ceramics. Curr. Opin. Solid State Mater. Sci. 2003, 7: 301.

Kajstura, J., Urbanek, K., Rota, M., Bearzi, C., Hosoda, T., Bolli, R., Anversa, P. & Leri, A. Cardiac stem cells and myocardial disease. J Mol Cell Cardiol 2008, 45(4):505-13.

Kak, A.C. & Slaney, M., Principles of Computerized Tomographic Imaging, Society of Industrial and Applied Mathematics, 2001.

Karageorgiou, V. & Kaplan D. Porosity of 3-D biomaterial scaffolds and osteogenesis. Biomaterials 2005, 26:5474–91.

Ketcham, R.A. & Carlson, W.D. Acquisition, optimization and interpretation of X-ray computed tomographic imagery: applications to the geosciences. Comput Geosci 2001, 27(4): 381–400.

Komlev, V., Mastrogiacomo, M., Pereira, R.C., Peyrin, F., Rustichelli, F., & Cancedda, R. Biodegradation of porous calcium phosphate scaffolds in ectopic bone formation model studied by X-ray computed microtomography. European Cells and Materials 2010, 19: 136-146.

Komlev, V., Mastrogiacomo, M., Peyrin, F., Cancedda, R., & Rustichelli, F. X-Ray Synchrotron Radiation Pseudo-Holotomography as a New Imaging Technique to Investigate Angio- and Microvasculogenesis with No Usage of Contrast Agents. Tissue Engineering: Part C 2009, 15(3): 425-430.

Komlev, V.S., Peyrin, F., Mastrogiacomo, M. , Cedola, A., Papadimitropoulos, A., Rustichelli, F., & Cancedda, R. 3D analysis by X-ray computed microtomography of in vivo bone growth into porous calcium phosphate scaffolds. Tissue Eng. 2006, 12: 3449-3458.

Kuboki, Y., Takita, H., Kobayashi, D., Tsuruga, E., Inoue, M., Murata, M., Nagai, N., Dohi, Y., & Ohgushi, H. BMP-induced osteogenesis on the surface of hydroxyapatite with geometrically feasible and nonfeasible structures: topology of osteogenesis. Journal of Biomedical Materials Research 1998, 39 (2):190–199.

Kudo, T., Fukuchi, K., Annala, A.J., Chatziioannou, A.F., Allada, V., Dahlbom, M., Tai, Y.C., Inubushi, M., Huang, S.C., Cherry, S.R., Phelps, M.E. & Schelbert, H.R. Noninvasive measurement of myocardial activity concentrations and perfusion defect sizes in rats with a new small-animal positron emission tomograph. Circulation. 2002,106:118-23.

Langer, R.S. & Vacanti, J.P. Tissue engineering: the challenges ahead. Sci. Am. 1999, 280:86.

Leri, A., Kajstura, J., Anversa P. & Frishman W.H. Myocardial regeneration and stem cell repair. Curr Probl Cardiol 2008, 33:91-153.

Li, Z., Lee, A., Huang, M., Chun, H., Chung, J., Chu, P., Hoyt, G., Yang, P., Rosenberg, J., Robbins, R.C. & Wu, J.C. Imaging Survival and Function of Transplanted Cardiac Resident Stem Cells. J Am Coll Cardiol 2009, 53:1229–40.

Mastrogiacomo, M., Komlev, V.S., Hausard, M., Peyrin, F., Turquier, F., Casari, S., Cedola, A., Rustichelli, F. & Cancedda, R.Synchrotron Radiation Microtomography of Bone Engineered from Bone Marrow Stromal Cells. Tissue Eng. 2004; 10: 1767.

Mastrogiacomo, M., Papadimitropoulos, A., Cedola, A., Peyrin, F., Giannoni, P., Pearce, S.G., Alini, M., Giannini, C., Guagliardi, A., & Cancedda R. Engineering of bone using bone marrow stromal cells and a silicon-stabilized tricalcium phosphate bioceramic. Evidence for a coupling between bone formation and scaffold resorption. Biomaterials 2007, 28: 1376.

Matsuura, K., Nagai, T., Nishigaki, N., Oyama, T., Nishi, J., Wada, H., Sano, M., Toko, H., Akazawa, H., Sato, T., Nakaya, H., Kasanuki, H. & Komuro, I. Adult cardiac Sca-1-positive cells differentiate into beating cardiomyocytes. J Biol Chem 2004; 279:11384-11391.

Menasche, P., Alfieri, O., Janssens, S., McKenna, W., Reichenspurrer, H., Trinquart, L., Vilquin, J., Marolleau, J.P., Seymour, B., Larghero, J., Lake, S., Chtellier, G., Solomon, S., Desnos, M. & Hagege, A. The Myoblast Autologous Grafting in Ischemic Cardiomyopathy (MAGIC) Trial.First Randomized Placebo-Controlled Study of Myoblast Transplantation. Circulation 2008;117:1189-1200.

Moore, M.J., Jabbari, E., Ritman, E.L.,. Lu, L.C, Currier, B.L., Windebank, A.J. & Yaszemski M.J. Quantitative analysis of interconnectivity of porous biodegradable scaffolds with micro-computed tomography. Journal of Biomedical Materials Research Part A 2004, 71A (2):258–267.

Murugan, R. & Ramakrishna, S. Nano-featured scaffolds for tissue engineering: a review of spinning methodologies. Tissue Engineering 2006, 12 (3):435–447.

Nuzzo, S., Peyrin, F., Cloetens, P., Baruchel, J. & Boivin, G. Quantification of the degree of mineralization of bone in three dimension using Synchrotron Radiation Microtomography. Med Phys 2002; 19: 2672-81.

Ohgushi, H., Goldberg, V.M., Caplan, A.I. Repair of bone defects with marrow cells and porous ceramic. Experiments in rats. Acta Orthop Scand 1989, 60(3): 334-9.

Okabe, M., Ikawa, M., Kominami, K., Nakanishi, T., Nishimune, Y. 'Green mice' as a source of ubiquitous green cells. FEBS Lett.1997, 407(3):313-9.

Oyama, T., Nagai, T., Wada, H., Naito, A.T., Matsuura, K., Iwanaga, K., Takahashi, T., Goto, M., Mikami, Y., Yasuda, N., Akazawa, H., Uezumi, A., Takeda, S. & Komuro, I. Cardiac side population cells have a potential to migrate and differentiate into cardiomyocytes in vitroand in vivo. J Cell Biol 2007; 176:329–41.

Papadimitropoulos, A., Mastrogiacomo, M. , Peyrin, F., Molinari, E., Komlev, V.S., Rustichelli, F., & Cancedda, R. Kinetics of In Vivo Bone Deposition by Bone Marrow Stromal Cells Within a Resorbable Porous Calcium Phosphate Scaffold:An X-Ray Computed Microtomography Study. Biotechnol. Bioeng. 2007, 98: 271.

Paulus, M.J., Gleason, S.S., Kennel, S.J., Hunsicker, P.R. & Johnson, D.K. High resolution x-ray computed tomography: an emerging tool for small animal cancer research. Neoplasia 2000; 2: 62-70.

Peyrin, F., Salomé, M., Cloetens, P., Laval-Jeantet, A.M., Ritman, E. & Ruegsegger, P., Micro-CT examinations of trabecular bone samples at different resolutions: 14, 7 and 2 micron level. Technol. Health Care 1998, 6: 391-401.

Reimer, P. & Weissleder, R. Development and experimental application of receptor - specific MR contrast media, Radiology 1996; 36: 153–163.

Salomé, M., Peyrin, F., Cloetens, P., Odet, C., Laval-Jeantet, A.M., Baruchel, J. & Spanne, P. A synchrotron radiation microtomography system for the analysis of trabecular bone samples. Med Phys 1999; 26: 2194-2204.

Schambach, S.J., Bag, S., Groden, C., Schilling, L., Brockmann, M.A., Vascular imaging in small rodents using micro-CT, Methods 2010, Volume 50, Issue 1, 26-35.

Schelbert, H.R., Inubushi, M. & Ross, R.S., PET imaging in small animals. J Nucl Cardiol, 2003, 10:513–20.

Shi, X.F., Sitharaman, B., Pham, Q.P., Liang, F., Wu, K., Billups , W.E., Wilson, L.J. & Mikos A.G. Fabrication of porous ultra-short single-walled carbon nanotube nanocomposite scaffolds for bone tissue engineering, Biomaterials 2007,28:4078–4090.

Silva, E.A. & Mooney, D.J. Spatiotemporal control of vascular endothelial growth factor delivery from injectable hydrogels enhances angiogenesis. J Thromb. Haemost. 2007, 5: 590.

Stokking, R., Zubal, I.G. & Viergever, M.A., Display of fused images: methods, interpretation, and diagnostic improvements. Semin Nucl Med, 2003, 33:219-227.

Terrovitis, J.V., Ruckdeschel Smith, R. & Marbán, E., Assessment and Optimization of Cell Engraftment After Transplantation Into the Heart. Circ. Res., 2010, 106:479-494.

Torrente, Y., Belicchi, M., Sampaolesi, M., Pisati, F., Meregalli, M., D'Antona, G., Tonlorenzi, R., Porretti, L., Gavina, M., Mamchaoui, K., Pellegrino, M.A., Furling, D., Mouly, V., Butler-Browne, G.S., Bottinelli, R., Cossu, G. & Bresolin, N. Human circulating AC133(+) stem cells restore dystrophin expression and ameliorate function in dystrophic skeletal muscle. J. Clin. Invest. 2004; 114:182– 195.

Torrente, Y., Gavina, M., Belicchi, M., Fiori, F., Komlev, V.S., Bresolin, N. & Rustichelli, F. High-resolution X-ray microtomography for three-dimensional visualition of human stem cell Muscle homing. Febs Letter 2006; 580: 5759-64.

Toyama, H., Ichise, M., Liow, J.S., Vines, D.C., Seneca, N.M., Modell, K.J. & Seidel, J. Green MV, Innis RB.Evaluation of anesthesia effects on [18F]FDG uptake in mouse brain and heart using small animal PET. Nucl Med Biol 2004, 31:251– 6.

Van Lenthe, G.H., Hagenmüller, H., Bohner, M., Hollister, S.J., Meinel, L. & Müller, R. Nondestructive micro-computed tomography for biological imaging and quantification of scaffold–bone interaction in vivo. Biomaterials 2007, 28 (15):2479–2490.

Villa, C., Erratico, S., Razini, P., Fiori, F., Rustichelli, F., Torrente, Y. & Belicchi, M., Stem Cell Tracking By Nanotechnologies, Int. J. Mol. Sci. 11 (2010) 1070-1081.

Wang, Y.X., Hussain, S.M. & Krestin, G.P. Superparamagnetic iron oxide contrast agents: application in MR imaging. Eur. Radiol. 2001, 11: 2319.

Webb, A. G., Introduction to Biomedical Imaging. IEEE Press Series on Biomedical Engineering Sponsored by the IEEE Engineering in Medicine and Biology Society Wiley-IEEE Press, 2003.

Weitkamp, T., Tafforeau, P., Boller, E., Cloetens, P., Valade, J.-P., Bernard, P., Peyrin, F., Ludwig, W., Helfen, L. & Baruchel, J., Status and evolution of the ESRF beamline ID19, AIP Conf. Proc., April 2010, Volume 1221, pp. 33-38.

Wellington, S.L. & Vinegar, H.J., X-ray computerized tomography. J Petr Techn 1987; 39(8): 885–98.

Williams, D., Benefit and risk in tissue engineering. Mater Today 2004; 7:24e9.

Wollert, K.C., Meyer, G.P., Lotz, J., Ringes-Lichtenberg, S., Lippolt, P., Breidenbach, C., Fichtner, S., Korte, T., Hornig, B., Arseniev, L., Hertenstein, B.,Ganser, A. & Drexler, H., Intracoronary autologous bone-marrow cell transfer after myocardial infarction: the BOOST randomised controlled clinical trial. Lancet 2004; 364:141– 8.

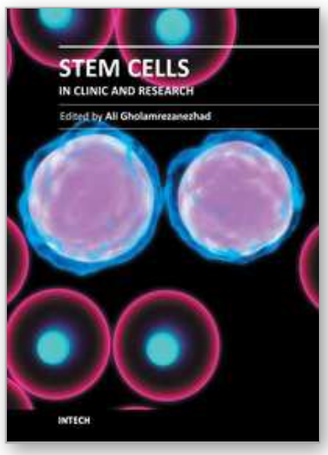

Stem Cells in Clinic and Research
Edited by Dr. Ali Gholamrezanezhad

ISBN 978-953-307-797-0
Hard cover, 804 pages
Publisher InTech
Published online 23, August, 2011
Published in print edition August, 2011

Based on our current understanding of cell biology and strong supporting evidence from previous experiences, different types of human stem cell populations are capable of undergoing differentiation or trans-differentiation into functionally and biologically active cells for use in therapeutic purposes. So far, progress regarding the use of both in vitro and in vivo regenerative medicine models already offers hope for the application of different types of stem cells as a powerful new therapeutic option to treat different diseases that were previously considered to be untreatable. Remarkable achievements in cell biology resulting in the isolation and characterization of various stem cells and progenitor cells has increased the expectation for the development of a new approach to the treatment of genetic and developmental human diseases. Due to the fact that currently stem cells and umbilical cord banks are so strictly defined and available, it seems that this mission is investigationally more practical than in the past. On the other hand, studies performed on stem cells, targeting their conversion into functionally mature tissue, are not necessarily seeking to result in the clinical application of the differentiated cells; In fact, still one of the important goals of these studies is to get acquainted with the natural process of development of mature cells from their immature progenitors during the embryonic period onwards, which can produce valuable results as knowledge of the developmental processes during embryogenesis. For example, the cellular and molecular mechanisms leading to mature and adult cells developmental abnormalities are relatively unknown. This lack of understanding stems from the lack of a good model system to study cell development and differentiation. Hence, the knowledge reached through these studies can prove to be a breakthrough in preventing developmental disorders. Meanwhile, many researchers conduct these studies to understand the molecular and cellular basis of cancer development. The fact that cancer is one of the leading causes of death throughout the world, highlights the importance of these researches in the fields of biology and medicine.

InTech Europe
University Campus STeP Ri
Slavka Krautzeka 83/A
51000 Rijeka, Croatia
Phone: +385 (51) 770 447
Fax: +385 (51) 686 166
www.intechopen.com

InTech China
Unit 405, Office Block, Hotel Equatorial Shanghai
No.65, Yan An Road (West), Shanghai, 200040, China
中国上海市延安西路65号上海国际贵都大饭店办公楼405单元
Phone: +86-21-62489820
Fax: +86-21-62489821

IntechOpen

IntechOpen